JOURNAL OF CATALYSIS 95, 546–557 (1985)

Structural Genesis of Pt on SiO_2: Determination by X-Ray Absorption Spectroscopy[1]

F. W. LYTLE,* R. B. GREEGOR,* E. C. MARQUES,†,[2] D. R. SANDSTROM,†,[3] G. H. VIA,‡ AND J. H. SINFELT‡

*The Boeing Company, Seattle, Washington 98124; †Department of Physics, Washington State University, Pullman, Washington 99164; and ‡Exxon Research & Engineering Co., Annandale, New Jersey 08801

Received December 12, 1984; revised June 3, 1985

Extended X-ray absorption fine structure (EXAFS) and X-ray absorption near-edge structure (XANES) were used to structurally characterize *in situ* a 1% Pt on Cab-O-Sil catalyst. We report data and structural parameters determined for a wide range of catalyst conditions varying from the dried, impregnated support to the sintered catalyst. Most of the work is on the active, clean catalyst and with chemisorbed O_2 and benzene. Specific new results include (1) evaluation of support interaction by measuring the Pt–O bonds to the support and by relating this to a residual, temperature-invariant static disorder, (2) the effect of chemisorbed O_2 or benzene, and (3) discovery of a temperature-driven change in the structure of the catalyst cluster believed to be due to making and breaking Pt–O bonds to the support. The effect was present either in H_2 or He. Sequential Fourier filtering in the data analysis with appropriately constructed phase shifts was used to uncover the minority-species-to-Pt bonds from the Pt–Pt bonds which predominate in the data.

INTRODUCTION

We used X-ray absorption spectroscopy combining X-ray absorption near edge structure (XANES) and extended X-ray absorption fine structure (EXAFS) to extensively characterize a 1 wt% Pt on Cab-O-Sil catalyst. XANES is the result of electron transitions to bound states of the absorbing atom and thereby maps the symmetry-selected empty manifold of electron states. It is sensitive to the electronic configuration of the absorbing atom. When the photoelectron has sufficient kinetic energy to be ejected from the atom it can be backscattered by neighboring atoms. Quantum interference of the initial electron wave state and backscattered wave produces a modulation of the absorption cross section. EXAFS data can provide information on bond distances, coordination numbers, disorder, and types of ligand for the first few coordination spheres. Although both XANES and EXAFS depend upon a measurement of X-ray absorption cross section the electronic and structural information is due to electron transitions and/or scattering where the source of electrons is an atomic species within the sample chosen by the coincidence in energy of the X-ray probe and the absorption edge of the element of interest. In this *element specificity* lies the power of the technique for catalyst characterization. Unlike most structural techniques, X-ray spectroscopy is not overwhelmed by the presence of the support. The support only appears in the data as it interacts with the catalytic atom. A recent review by Lee *et al.* has discussed the general use of the EXAFS technique and its limitations (*1*). We have reviewed catalytic applications (*2, 3*) of both EXAFS and XANES.

[1] A preliminary version of this paper was presented at the conference, Advances in Catalytic Chemistry II, Salt Lake City, May (1982).

[2] Present address: Monsanto Co., 800 N. Lindbergh, St. Louis, Mo. 63166.

[3] Present address: The Boeing Co., P.O. Box 3999, Seattle, Wash. 98124.

0021-9517/85 $3.00

In the following we obtain structural data for Pt atoms and their first neighbors during the process of catalyst genesis from the impregnated support, through reduction, O_2 and benzene chemisorption, and investigation of structural changes with temperature. We measured both the thermal and static disorder, relating the latter to a support effect. We also note a new effect with increasing temperature in H_2 or He, i.e., the XANES changes reversibly with temperature in a manner which suggests a change in shape of the catalyst cluster. We attempt to place these new results within the context of previous work and discuss the significance of the new or differing results. Connecting all these bits and pieces of evidence helped provide considerable insight and detail for the total preparation of this catalyst—a structural genesis. To complement these results consult the outstanding series of papers by Cohen, Butt, Burwell, and collaborators (*4–7*) who have used chemical techniques, X-ray diffraction, and some EXAFS (*7*) to characterize Pt/SiO_2 catalysts with a wide range of dispersion (0.06–0.8).

Lagarde *et al.* have used the EXAFS technique to investigate Pt/Al_2O_3 catalysts in the form of the dried, impregnated support ($PtCl_6$ coordination), after calcination at 500–700°C (Pt–O and Pt–Cl coordination) and after reduction in H_2 at 480°C. They found that the reduced Pt clusters are in the normal fcc coordination with some Pt–O bonds to the support (*8, 9*).

EXPERIMENTAL METHODS

The preparation and characterization by chemisorption (H/Pt = 0.9) of the 1 wt% Pt on Cab-O-Sil has been described (*10*). The data were obtained in the catalyst cell shown in Fig. 1 either by transmission measurements, ($\ln I_0/I$), or by the fluorescent EXAFS technique (*11*) (I_F/I_0) where I_0, I, and I_F are the intensity of the incident X rays, transmitted X rays, and Pt L_α fluorescent X rays, respectively. The cell in Fig. 1 is similar to an earlier one (*2*) but with provision for measuring the fluorescent X rays. For Pt at 1% concentration the transmission and fluorescent techniques are about of equal merit. The fluorescent EXAFS technique becomes advantageous for elements of lower atomic number or at lower concentration (to 10 ppm in favorable cases). The measurements were made at Stanford Synchrotron Radiation Laboratory. In all cases a Si(220) double-crystal monochromator was used with entrance slit (1 mm high and 20 m from the source point) chosen to give a bandpass of 2 eV at the Pt L_{III} edge, 11,563.7 eV (*12*). The operation of the catalyst cell allowed *in situ* reduction, chemisorption, and catalysis while maintaining the temperature in the desired range from 90 to 1300 K. In practice, once a desirable catalyst condition was achieved X-ray measurements often were taken at temperature and then after quenching to 90 K in an attempt to minimize thermal smearing of the EXAFS data. For each measurement typically 2 to 3 scans were averaged over a total time of ~40 min. Temperatures were measured by the thermocouple indicated in Fig. 1 and kept constant at the temperatures indicated to ±5°C. For all the analysis that follows we used only the Pt L_{III} XANES and EXAFS. Note the sharp XANES feature at the L_{III} edge which will become more evident later when the graph is expanded.

The object of these experiments was to demonstrate the sensitivity of the technique with the same model catalyst under a number of different conditions. The somewhat cryptic legend in Fig. 2 describes the catalyst condition achieved before the catalyst was quenched to 90 K for a data scan. The XANES and accompanying EXAFS data are given in Figs. 2 and 3. Sample A was the original $H_2PtCl_6 \cdot 6H_2O$-impregnated Cab-O-Sil support air-dried at 383 K. The XANES/EXAFS was very similar to that of solid $H_2PtCl_6 \cdot 6H_2O$ and the measured Pt–Cl bond distance from a phase-corrected Fourier transform was 2.35 Å compared to 2.32 Å of the parent compound

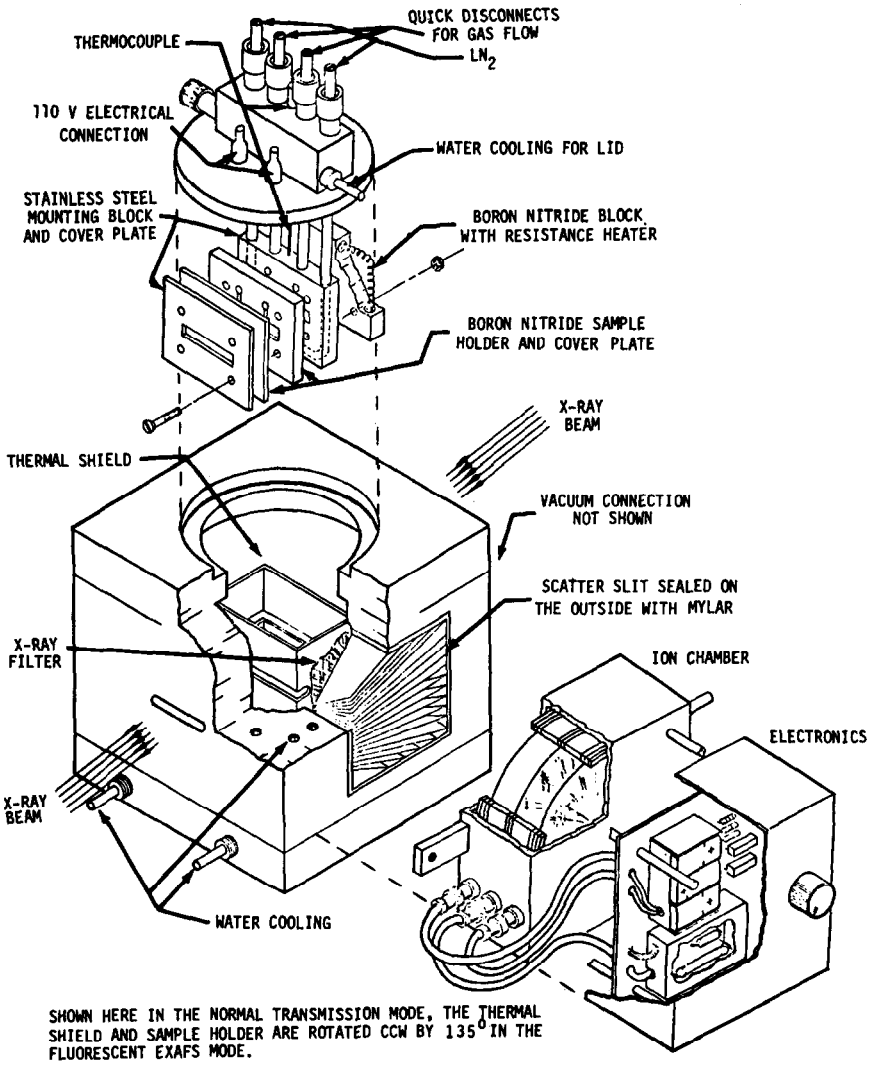

FIG. 1. Continuous-flow catalyst cell for X-ray absorption spectroscopy. The principles of operation have been described (*2, 10*).

indicating Cl coordination as was also found by Lagarde *et al.* (*8*). This preparation was not investigated further. One sample was sintered by calcining in air at 1073 K to produce sample E. There was little difference in the data between this and metallic Pt, as expected, since the particle size was ~200 Å. This preparation was not investigated further. Parenthetically, we note that a world of significant chemistry and crystallography occurs and could be measured between sample A and B or A and E. For now we choose to emphasize the reduced catalyst and reactions thereon. For all the following preparations the catalyst cell was operated in a flow condition into ambient pressure. Sample B was prepared from A by reduction in flowing H_2 for 4 h at 773 K. Then, during cooling, He was used to sweep away the H_2 and the catalyst was passivated by gradual exposure to air. The air-exposed catalyst was stored in a sample bottle until ready for use at SSRL. It was then rereduced at 773 K in flowing H_2 *in*

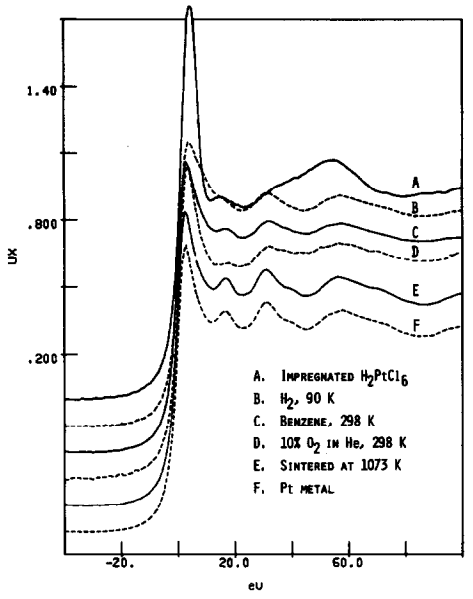

FIG. 2. Platinum L_{III} absorption edges of 1% Pt on Cab-O-Sil in various chemical conditions compared to Pt metal. All are plotted to the same scale. See Figs. 11a and b for expanded views of the near-edge region.

situ in the apparatus shown in Fig. 1. Data were taken as a function of temperature during cooling in H_2 to an ultimate low temperature of 90 K (sample B). The determination of disorder as a function of temperature and of an interaction with the support will be described later. Samples C and D were prepared by heating to 773 K in H_2, cooling in He, and then initiating a flow of He + benzene vapor or 10% O_2 in He at 298 K. After equilibration the pure-He flow was restarted and the sample cooled to 90 K for measurement. Note the sensitivity of the near-edge peak in Fig. 2 to the condition of the catalyst. (This data is examined in more detail in Figs. 11a and b.) The EXAFS of Fig. 3 corresponds to the XANES of Fig. 2, each measured at 90 K after achieving the desired catalyst condition. Note that the Pt–Cl ligation in A produces EXAFS plainly different than all the other samples which have primarily Pt–Pt bonds. The well-dispersed catalysts (B, C, and D) have smaller amplitude than E and F because of their smaller average coordination number.

EXAFS DATA ANALYSIS

We have described in detail our technique of data analysis (*2, 10*). Basically, the EXAFS, $\chi(K)$

$$\chi(K) = \sum_j A_j(K) \sin[2KR_j + \phi_j(K)] \quad (1)$$

$$A_j(K) = (N_j/KR_j^2)F_j(K) \exp(-2K^2\sigma_j^2) \quad (2)$$

is Fourier-transformed

$$\Phi_n(R) = (1/2\pi)^{1/2} \int_{K_{min}}^{K_{max}} K^n\chi(K) \exp(2iKR)\, dK \quad (3)$$

to produce a radial structure function centered on the absorbing atom. We proceed by taking the inverse transform of the first-neighbor peak and then extract the unknown functions $F_j(K)$, electron backscattering, and $\phi_j(K)$, phase shift, from Pt metal as a reference. Then by a least-squares fitting routine we evaluate N_1, R_1, and $\Delta\sigma_1^2$ for

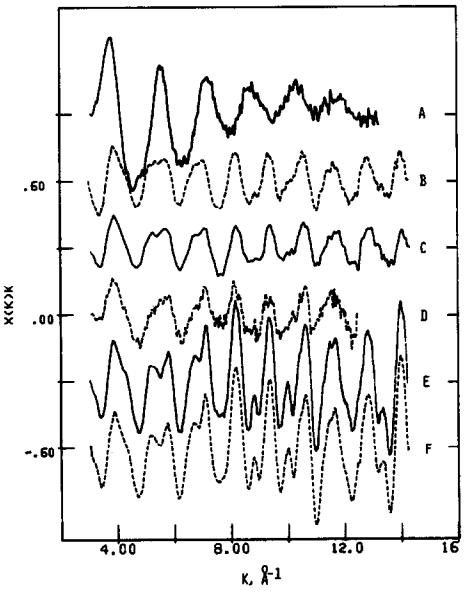

FIG. 3. EXAFS spectra corresponding to the near-edge spectra shown in Fig. 2. See the legend in Fig. 2 for identification. The position of the ordinate scale applies to spectrum D; however, all are plotted to the same scale. The spectra of Figs. 2 and 3 were all measured at 90 K after conditioning the catalyst as indicated.

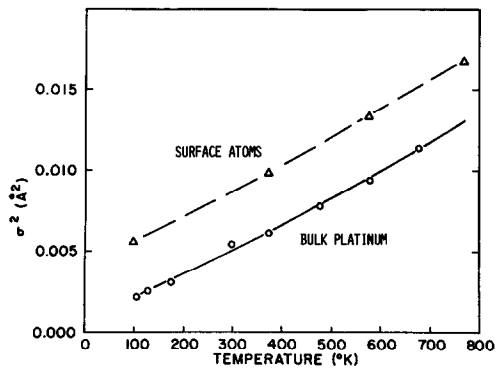

FIG. 4. Comparison of relative mean squared thermal motion for bulk and surface Pt atoms as a function of temperature. The triangles mark the catalyst surface atoms; the circles are for bulk Pt.

the catalyst. (The $\Delta\sigma_1^2$ is the increase in disorder over Pt metal at the temperature of measurement, 90 K.) We found for the Pt–Pt bonds $N_1 = 8 \pm 1.5$, $R_1 = 2.77 \pm 0.01$ Å, and $\Delta\sigma_1^2 = 0.0018$ Å^2 (*10*).

In a recent paper we used a temperature sequence of EXAFS measurements of the reduced catalyst in H_2 to investigate the temperature dependence of the disorder (*14*). The pertinent results are given in Fig. 4 and show that the relative thermal motion of the surface atoms is significantly greater than in the bulk metal over the range 100–800 K. This result was expected considering the partial coordination, hence lack of constraint of the surface atoms. A similar result has been found from LEED measurements on single-crystal Pt (*15*). We believe it is significant that disorder when extrapolated to 0 K remains considerably larger than for bulk Pt. This indicates a significant static disorder. Related measurements have been made by Sashital *et al.* (*5*) using X-ray diffraction. Their technique determined the average mean squared displacement at 298 K of all the atoms in the cluster, not just the surface atoms, in catalysts with dispersion varying from 0.06 to 0.4. Allowing for the difference in disperison their results for σ^2 are comparable to those given in Fig. 4. They found unstrained, spherical metal clusters (*5*) with little contact to the support (*7*) whereas we found a static disorder in addition to the thermal effect which we interpret as strain caused by Pt–O bonds to the support (discussed in detail later). These apparent discrepancies may be due to the difference in dispersion, hence the different size and shape, between their catalysts and ours. We found a mixture (*13*) of raft-like and sphere-like shapes with a mean diameter of 10–15 Å which would indicate a considerable contact area with the support whereas their catalysts were >25 Å and spherical in shape. We believe the formation of raft-like shapes in very small clusters is mediated by Pt–O bonds to the support.

SEQUENTIAL FOURIER FILTERING WITH PHASE SHIFT

The effect of including the phase shift in the transform of Pt EXAFS data was previously shown by Marques *et al.* (*14*). This results in a very useful sharpening and simplification of the peaks of the Fourier transform, particularly in those elements such as Pt which have phase shifts which are very nonlinear. Equation (3) is modified by including the phase shift, $\phi(K)$,

$$\Phi_n(R) = (1/2\pi)^{1/2} \int_{K_{\min}}^{K_{\max}} K^n \chi(K) \exp[i[2KR + \phi_j(K)]]\, dK. \quad (4)$$

The effect is quite marked as shown by the K^1 transforms in Fig. 5. The phase shift makes the full range of $\chi(K)$ periodic in K and thereby "focuses" the transform. The effect is particularly dramatic for the catalyst data. Inclusion of the phase shift locates the Pt–Pt peaks at their correct distances. The measured (known) radial distances of the first through fifth coordination spheres for bulk Pt at 90 K are 2.769 (2.769), 3.948 (3.917), 4.803 (4.797), 5.537 (5.539), and 6.172 (6.193) Å, respectively. Note that in the phase-corrected transform of the catalyst there is still a smeared area near 2 Å. This was analyzed further below and shown in Fig. 9.

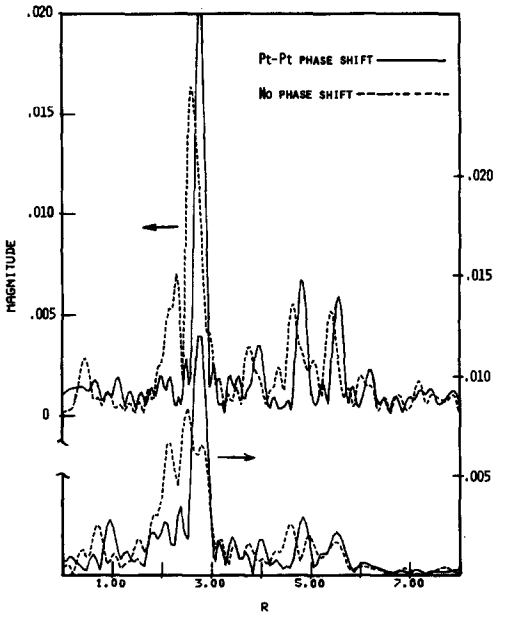

FIG. 5. The effect of including the Pt–Pt phase during the Fourier transform of EXAFS data for (top) Pt metal (F in Fig. 3) and (bottom) the reduced Pt catalyst (B in Fig. 3).

A very good approximation of $\phi_j(K)$ may be obtained from the tables of Teo and Lee (*16*) or may be more precisely determined from a reference compound as follows. The total phase

$$\phi_{\text{total}}(K) = 2KR + \phi_j(K) \qquad (5)$$

was evaluated from the "no phase shift" Fourier transform. In the top, dashed transform of Fig. 5, the harmonics below ~1.5 Å and above ~3.5 Å were zeroed out and the inverse transform performed.

$$K^n X_1(K) = (2/\pi)^{1/2} \int_{R_1-\Delta R}^{R_1+\Delta R} \Phi_n(R) \exp[-(2iKR)]\, dR. \qquad (6)$$

This complex transform has real, Re(K) and imaginary Im(K) parts. Then

$$\phi_{\text{total}}(K) = \tan^{-1}[\text{Im}(K)/\text{Re}(K)]. \qquad (7)$$

This function is shown in Fig. 6. The desired phase shift function results from the simple subtraction

$$\phi_j(K) = \phi_{\text{total}}(K) - 2KR_j, \qquad (8)$$

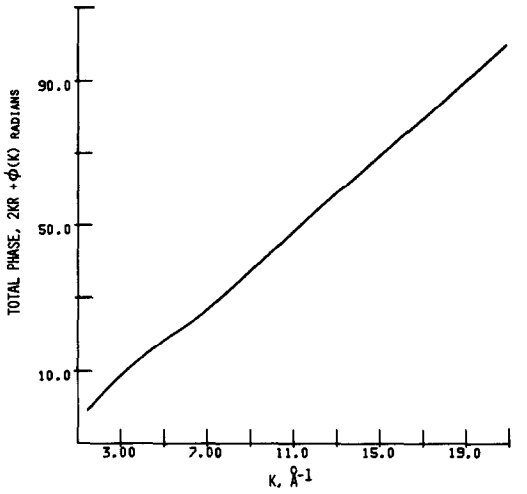

FIG. 6. Total phase, ϕ_{total} (K) for Pt metal at 90 K.

where R_j is the accurately known distance for the radial structure peak. For Pt at 90 K, R_1 = 2.769 Å and the resulting phase shift $\phi_{\text{Pt–Pt}}(K)$ is shown in Fig. 7. This function was used to obtain the solid-line transforms of Figs. 5, 9, and 10. In these catalysts which have primarily Pt–Pt bonds this phase shift gives sharp peaks wherever Pt–Pt bonds are present. The variation in $F(K)$ and $\phi(K)$ with chemical or surface state was not investigated, i.e., we extracted these quantities from model compounds;

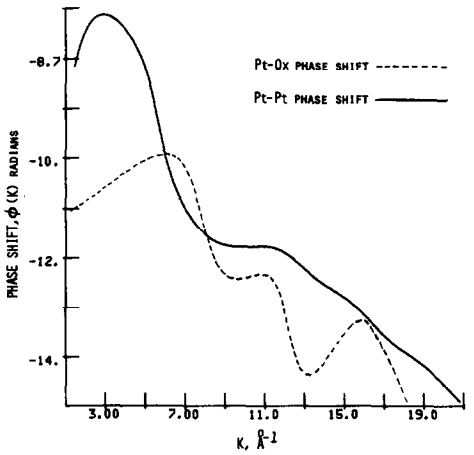

FIG. 7. Solid line: Pt–Pt phase shift evaluated from the "no phase shift" transform of Fig. 5 with R_1 = 2.769 Å. Dashed line: Pt–Ox phase shift evaluated as described in the text with R_1 = 2.07 Å.

TABLE 1

Summary of Measured Parameters for 1% Pt on Cab-O-Sil Catalyst

Catalyst	Significant parameters
Air-dried, $H_2PtCl \cdot 6H_2O$ impregnated	Pt–Cl same as in $H_2PtCl_6 \cdot 6H_2O$
Reduced in H_2, measured at 90 K	N_1(Pt–Pt) ~ 8, R_1(Pt–Pt) = 2.77 Å N_1(Pt–O) ~ 0.5, R_1(Pt–O) = 1.91 Å Size = 10–15 Å diameter mix of disks and polyhedra
Chemisorbed O_2, 298 K	N_1(Pt–O) ~ 2, R_1(Pt–O) = 2.03 Å
Chemisorbed benzene, 298 K	N_1(Pt–C), R_1(Pt–C) presence indicated but not yet measured accurately
Reduced in H_2, measured from 90 to 800 K in H_2 or He	Disorder of surface atoms = 1.3–2 times bulk Pt. *d*-Electron concentration increases with temperature
Sintered at 1073 K, measured at 90 K	Catalyst particles so large that EXAFS/XANES same as bulk Pt

however, the topic should be discussed. As shown by the calculations of Teo and Lee (*16*) these effects become more important for low-atomic-number backscattering elements and even then are relatively small. Thus we expect the Pt–Pt bonds to be very well described including the residual static disorder but with less certainty for Pt–O or Pt–C bonds. (The effect would become important for quantitatively separating Pt–O and Pt–C bonds which we have not attempted here.) Within the accuracy requirements of this study the effect of a surface location or a valence different from the reference compound is not expected to change our conclusions. The uncertainty is indicated by the error bars in Table 1. We next demonstrate selective filtering in order to measure other bond types in cases of complex coordination.

We used α-PtO_2 which has a CdI_2 type of structure (*17*) with six first-neighbor oxygen atoms at 2.07 Å and second-neighbor Pt atoms to evaluate a Pt–Ox phase shift. In Fig. 8 the "no phase shift" curve shows a broadened Pt–O peak and a complicated second-neighbor Pt–Pt peak. When transformed with the Pt–Pt phase shift this peak becomes very sharp but the Pt–O peak is smeared, mainly toward the left and does not mix appreciably with the Pt–Pt peak. Next, we took the inverse transform of this smeared Pt–O peak including harmonics from ~0.5 to 2.9 Å, evaluated the total phase, and subtracted $2KR_1$ where R_1 = 2.07 Å, the known Pt–O distance. The resulting Pt–Ox phase shift is shown by the dashed curve in Fig. 7. This complicated function is *not* the normal Pt–O phase shift but a convoluted sum which includes the Pt–Pt phase shift also. It is applied only to inverse transforms after a Pt–Pt phase shift has already been applied. The effect on the extracted phase caused by the range in R of

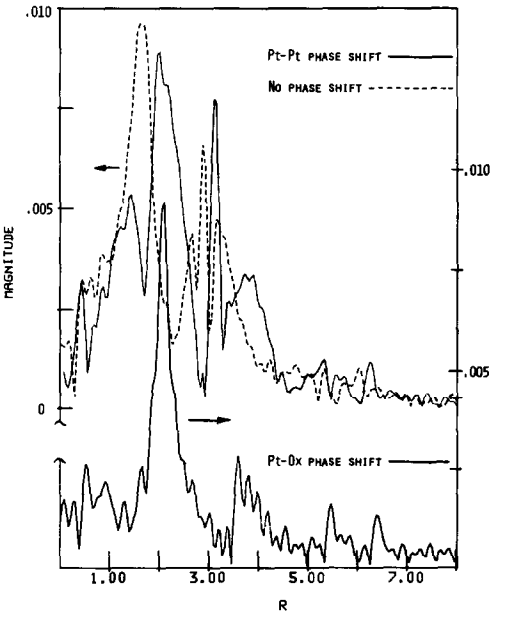

FIG. 8. Fourier transforms of PtO_2 EXAFS data illustrating the inclusion of the phase shift during the transform and sequential Fourier transforms. The dotted line in the top part of the figure shows the transform without a phase shift, the solid line shows the transform with the correct phase shift for Pt–Pt bonds. The second-neighbor Pt–Pt peak near 3.2 Å is now in sharp "focus." After selectively filtering out the Pt–Pt peak at 3.2 Å the Pt–Ox phase shift was applied as described in the text to give the bottom curve.

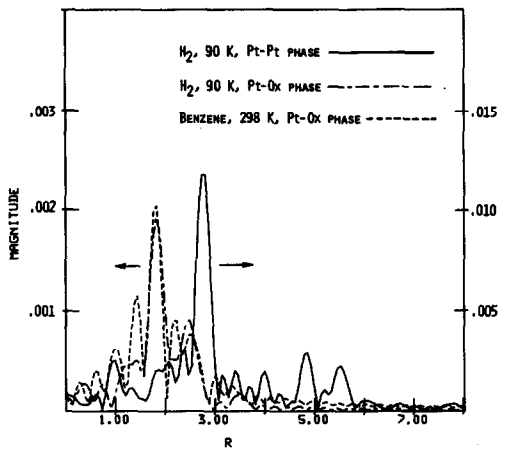

FIG. 9. The solid line shows the transform when the Pt–Pt phase shift has been applied. (Note that the scale of all the Pt–Pt transforms has been kept the same as Pt metal.) Then after zeroing harmonics above ~2.5 Å and inverse transforming the Pt–Ox phase shift was applied to obtain the dashed-line transforms. The reduced catalyst B has a Pt–O strong peak at 1.91 Å. The benzene catalyst C has the Pt–O peak plus additional peaks due to Pt–C bonds smeared by the Pt–Ox phase shift.

the inverse transform was investigated. As long as the major sidelobe on each side of the peak of interest was included the extracted phase was invariant within the requirements of this paper. The sequential filtering on catalysts to remove the Pt–Pt bonds was not always completely "clean." Note the leakage of Pt–Pt bonds in the dashed curve in Fig. 10 but note that it does not interfere with the Pt–O bond. In Fig. 8 (bottom part), this was done to the inverse transform of the solid-line function at the top where the Pt–Pt peak has been filtered out to prevent smearing. The result is a sharp first-neighbor peak at the correct Pt–O bond distance. We now use this Pt–Ox phase shift to investigate Pt–O bonds to the support (catalyst B) and to chemisorbed O_2 (catalyst D). The data analysis sequence proceeded by transforming with the Pt–Pt phase shift, zeroing out harmonics above ~2.5 Å, taking the inverse transform, then retransforming with the Pt–Ox phase shift. The results are shown by the dashed curves in Figs. 9 and 10. In each the smear of harmonics to the left of the Pt–Pt peak has been focused by the Pt–Ox phase shift into a sharp Pt–O peak. In catalyst B after reduction in H_2 and cooling to 90 K this peak was at R = 1.91 Å. The intensity of the peak compared to that of PtO_2 suggests approximately one-half oxygen neighbor per Pt atom. The same catalyst with benzene chemisorbed has the same peak plus others due to Pt–C bonds. We expect Pt–O and Pt–C bond distances to be sufficiently similar to preclude further selective filtering. However, least-squares fitting of that region of the transform should be possible. It has not yet been attempted here for want of data on a suitable reference compound with Pt–C bonds. Catalyst D with chemisorbed O_2 is shown in Fig. 10. Here the Pt–Pt peak is broadened and diminished in intensity because of increased disorder in the Pt cluster induced by the O_2 chemisorption. After sequential filtering and application of the Pt–Ox phase shift the primary peak was found at R = 2.03 Å and was approximately 0.4 times as intense as that of PtO_2 or approximately 2 Pt–O bonds for the average Pt atom. The double peak is probably a result of the fairly noisy data. The remanent Pt–Pt

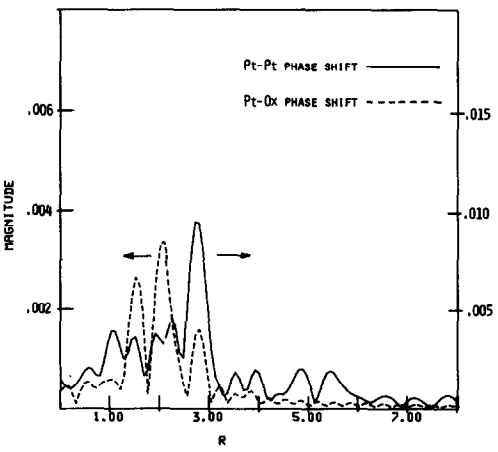

FIG. 10. The solid line shows catalyst D with Pt–Pt phase shift. The dashed line is the result of the double-filtering procedure with the final transform using the Pt–Ox phase shift. The major Pt–O peak is at 2.03 Å.

bonds in the catalyst exposed to O_2, which are probably in the core of larger clusters, agrees with EXAFS results of Nandi *et al.* (*7*). Also by X-ray diffraction they identified the platinum oxide phase as Pt_3O_4.

ANALYSIS OF XANES DATA

The electronic dipole transition at the Pt L_{III} edge is from the $2p_{3/2}$ core level to the empty 5*d* and 6*s* state; however, the transition to 6*s* has a much lower probability and is not expected to contribute measurably. In previous work (*18*) it was shown that the intensity of the peak at the L_{III} absorption edge was proportional to the *d*-electron vacancies. A series of compounds of one element illustrated that the increase in the peak intensity of the compound compared with the pure element was proportional to an ionicity estimate of the number of 5*d* electrons removed from the element by formation of chemical bonds (*19*). In this same work XANES sensitivity to interaction with the support and to O_2 chemisorption was also demonstrated for Pt and Ir supported on Al_2O_3. Gallezot *et al.* (*20*) demonstrated similar effects for Pt on zeolites. Mansour *et al.* (*21*) investigated Pt on SiO_2 and Al_2O_3 as a function of H_2 reduction temperature. All three studies (Refs. (*19–21*)) agreed that the increase in area of the peak at the Pt *L* edge(s) indicated that supported Pt was electron deficient. The most simple explanation is that Pt 5*d* electrons form bonds with available ligands on the support. Short *et al.* (*22*) have used the same technique to explore the strong metal–support interaction (*23*) (SMSI) of Pt on TiO_2. A small effect was noted on the EXAFS and XANES between the normal and SMSI catalyst conditions. An interesting result in light of Refs. (*19–21*) was that the L_{III} edge peak was diminished in intensity and width compared to bulk Pt in contrast with the particularly wide feature observed on SiO_2 or Al_2O_3. A serious caveat of all the above results (Refs. (*19–22*)) is that the catalyst was conditioned at a particular temperature and then cooled to room temperature or below for the X-ray measurement. We have found a significant temperature effect on the XANES of a Pt catalyst in H_2 or He which is discussed below. Recently, Horsley (*24*) has shown how the $L_{II,III}$ X-ray absorption edge resonances can be modeled by $X\alpha$-SW molecular orbital calculations of a cluster composed of Pt or Ir and its first neighbors. There was good agreement with experiment. Both Horsley (*24*) and Mansour *et al.* (*21*) showed that the L_{III} and L_{II} edges must both be considered for a quantitative measure of *d*-state occupancy.

The expanded views of the Pt L_{III} edge shown in Figs. 11a and b and the difference spectra of Fig. 12 were measured *in situ* at the temperature and under the conditions indicated. The curve for 1% Pt in H_2 at 90 K is similar to those published previously (*19, 21*). The interesting new result is the diminished, narrower peak at high temperature. There is a gradual transition with temperature from the broad low-temperature peak to the narrow high-temperature peak. This change is shown in Fig. 13 by plotting the difference area versus absolute temperature. The difference area was defined as the first major peak resulting from the subtraction of the highest temperature spectrum from the lower temperature spectra using the procedure described previously (*19*). Note that the trend is the same either with increasing or decreasing temperature. Examples of difference spectra appear in Fig. 12. The normal L_{III} absorption spectrum of bulk Pt is overdrawn as a guide to the eye in identifying the active regions of the spectra. The difference peak of interest is the first one peaking at 2–8 eV, approximately. We identify this peak with transitions to empty *d*-states and use its area as a measure of *d*-electron vacancies. The wiggles at higher energy are due to EXAFS differences and oscillate about the zero line showing that the normalization of the spectra was accurate. Note that the active region during chemisorption of O_2 or benzene

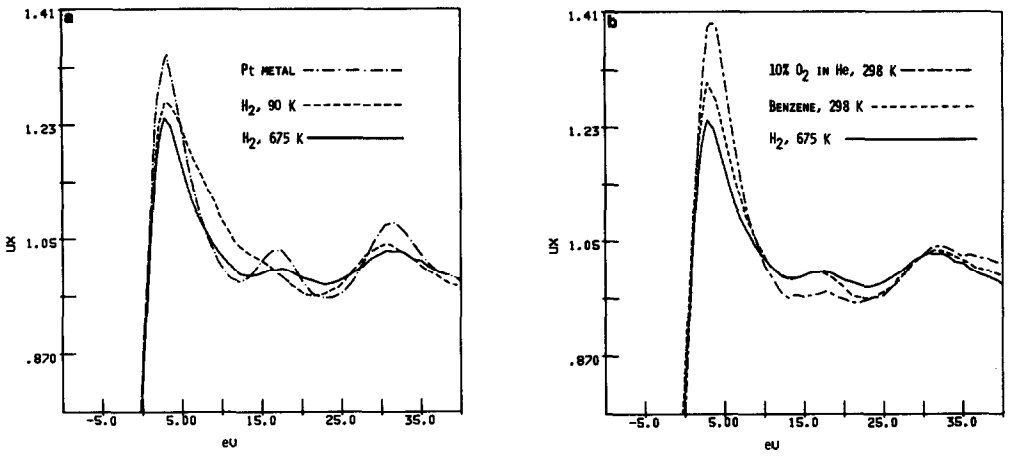

FIG. 11. (a,b) Expanded region of near-edge spectra. Note the sensitivity of the first absorption maxima to the catalyst environment. These spectra were subtracted in various combinations to produce the difference spectra of Fig. 12. Note that these spectra were measured at the temperatures indicated.

occurs at the peak of the absorption edge, approximately 4 eV above the inflection point (Fermi surface). The difference spectrum of the low-temperature catalyst forms a peak at approximately 8 eV and is due to a filling in on the high-energy side of the L_{III} peak. This energy dependence suggests that different orbitals or different mechanisms are involved. Clearly there is evidence of a change in the *d*-electron states of the Pt atom with temperature. This effect has been investigated in more detail with a 0.5 wt% Pt on Cab-O-Sil catalyst of higher dispersion ($D = 1.0$) (*25*). It was shown that the effect was present for both the Pt L_{II} and L_{III} edges and was present in both H_2 and He. We believe the most likely explanation to be due to making and breaking Pt–O bonds to the support. Preliminary calculations (*25*) show that Pt 5*d*-orbitals interact with O 2*p*-orbitals to create a hybrid orbital with bonding and antibonding

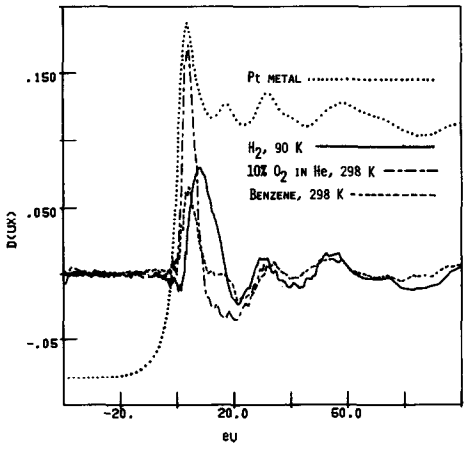

FIG. 12. Difference spectra where the H_2, 675 K spectrum has been subtracted from the data as indicated. The dotted absorption edge of Pt metal is shown as a guide to the eye.

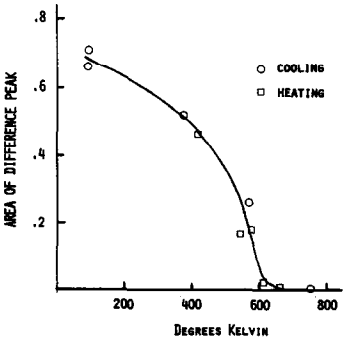

FIG. 13. Area of the first peak in difference curve of the Pt L_{III} edge versus absolute temperature for 1% Pt on Cab-O-Sil in H_2. The high-temperature measurement (773 K) was subtracted from each of the other spectra.

states below and above the Pt *d*-band, respectively. The increased X-ray absorption at low temperature is due to transitions to the empty antibonding orbitals. At high temperatures the Pt–O bonds to the support break because of increased thermal motion and the antibonding orbitals disappear. The cluster probably "curls up" to a more nearly spherical shape. Presumably, at even higher temperatures where the catalyst sinters, all the Pt–O bonds break and the clusters become mobile, thereby suggesting a model for agglomeration and sintering.

In Fig. 6 of Ref. (*19*) the difference area of a series of compounds were related to a "coordination charge" through an argument using the Pauling electronegativities of the reacting atoms. Horsley's work (Fig. 3 in Ref. (*24*)) suggests that multiplying the coordination charge by 2 approximately converts it to a *d*-vacancy scale. For the present work this conversion was made to very qualitatively assess the changes in the Pt *d*-electrons of the catalyst compared to bulk Pt. We estimate that the average Pt atom on the catalyst gains 0.1 electrons upon heating in H_2 or He. Each Pt atom loses 0.4 or 0.1 electrons during chemisorption of O_2 and benzene, respectively. Using PtO_2 with six oxygen neighbors as a reference [1.5 *d*-electron vacancies (*24*)] this represents 1.6 oxygen ligands per Pt atom in rough agreement with the EXAFS result. A suitable reference was not available for the Pt–C bond.

DISCUSSION

The EXAFS and XANES measurements are complementary. EXAFS detects the presence of nearby atoms, XANES measures the changes in electron concentration. Since this XANES effect depends upon the relative electronegativity of the atom and its ligands, its sensitivity will be ligand dependent. For example, a Pt–O bond is much easier to detect than Pt–C. For EXAFS the total number of electrons on the atom is the important backscattering variable, i.e., H is essentially invisible. When processing EXAFS data the use of Fourier transforms with a phase shift followed by selective filtering were very useful data manipulation techniques. It was possible to obtain clean separation of previously interfering bonds which aided in the evaluation of their parameters.

The primary new result of this paper is the temperature effect discovered for Pt in H_2 and He (*25*) and its relationship to Pt–O bonds to the support. It is interesting and may be significant since it is under the high-temperature condition with excess H_2 that Pt catalysts are usually used for hydrocarbon chemistry. The low-temperature state previously measured (*19, 21*) is plainly different from high-temperature catalyst. The *L*-absorption peaks indicate that the Pt catalyst in H_2 (or He) appears to add ~0.1 electrons per atom (compared to the bulk) with increasing temperature, saturated above 600 K. The diminished L_{III} edge peak of the high-temperature form must be due to size or shape effects inherent in small, spherical clusters. (We have verified that there is no measurable temperature effect in bulk Pt over this range.) Without proving it we suggest that the measured Pt–O bonds to the support create lattice strains which are the cause of the high static disorder. Similarly, thermally breaking these Pt–O bonds results in a change of shape of the cluster, probably to a more spherical form. The fact that Pt on TiO_2 (*22*) has a narrow absorption edge at low temperature in both the normal and SMSI states may be a related effect. (The high-temperature state of Pt on TiO_2 has not yet been measured.) EXAFS data of sufficient quality could help answer some of these questions by way of the shape effect (*13*); however, thermal smearing is a serious problem (which is the reason why most of the data (*19, 21*) were recorded at low temperature).

The summary of measured parameters for this catalyst, contained in Table 1, is a wealth of direct structural information. Given the perspective of a few years' expe-

rience the degree of detail is remarkable. Many parameters have now been confirmed by other groups (*7–9, 20–22*) and must be considered to be valid. Small Pt clusters on SiO_2 are very much like bulk Pt in many respects. The atoms appear to pack in the same way with the same bond distance, the reduced coordination number is a result of their small size. In very small clusters there is a significant static and dynamic increase in the disorder compared to bulk Pt. The static disorder is probably due to strains induced by bonds to the support. The increased dynamic disorder is due to the large fraction of surface atoms and their inherent flexibility. It may prove possible to connect this parameter with reaction kinetics (*7, 14*). Pt on SiO_2 in H_2 or He may be either in an electron-deficient or surplus condition depending on temperature. This fact may have implications for the applications of Pt catalysts.

ACKNOWLEDGMENTS

The work of R. B. Greegor, F. W. Lytle, E. C. Marques, and D. R. Sandstrom was supported by the National Science Foundation, Grant CHE 82-19605. The X-ray measurements were made at the Stanford Synchrotron Radiation Laboratory which was supported by the DOE.

REFERENCES

1. Lee, P. A., Citrin, P. H., and Kincaid, B. M., *Rev. Mod. Phys.* **53,** 769 (1981).
2. Lytle, F. W., Via, G. H., and Sinfelt, J. H., "X-Ray Absorption Spectroscopy: Catalyst Applications" *in* Synchrotron Radiation Research (H. Winick and S. Doniach, Eds.), p. 401. Plenum, New York, 1980.
3. Sinfelt, J. H., Via, G. A., and Lytle, F. W., *Catal. Rev.* **26,** 81 (1984).
4. Uchijima, T., Herrmann, J. M., Inous, Y., Burwell, R. L., Jr., Butt, J. B., and Cohen, J. B., *J. Catal.* **50,** 464 (1977).
5. Sashital, S. R., Cohen, J. B., Burwell, R. L., Jr., and Butt, J. B., *J. Catal.* **50,** 479 (1977).
6. Otero-Schipper, P. H., Wachter, W. A., Butt, J. B., Burwell, R. L., Jr., and Cohen, J. B., *J. Catal.* **50,** 494 (1977).
7. Nandi, R. K., Molinaro, F., Tang, C., Cohen, J. B., Butt, J. B., and Burwell, R. L., Jr., *J. Catal.* **78,** 289 (1982).
8. Lagarde, P., Murata, T., Vlaic, G., Freund, E., Dexpert, H., and Bournonville, J. P., *J. Catal.* **84,** 333 (1983).
9. Dexpert, H., and Lagarde, P., *J. Mol. Catal.* **25,** 347 (1984).
10. Via, G. H., Sinfelt, J. H., and Lytle, F. W., *J. Chem. Phys.* **71,** 690 (1979).
11. Jaklevic, J., Kirby, J. A., Klein, M. P., Robertson, A. S., Brown, G. S., and Eisenberger, P., *Solid State Commun.* **23,** 679 (1977).
12. Bearden, J. A., and Burr, A. F., *Rev. Mod. Phys.* **39,** 125 (1967).
13. Greegor, R. B., and Lytle, F. W., *J. Catal.* **63,** 476 (1980).
14. Marques, E. C., Sandstrom, D. R., Lytle, F. W., and Greegor, R. B., *J. Chem. Phys.,* July 15 (1982).
15. Lyon, H. B., and Somorjai, G. A., *J. Chem. Phys.* **44,** 3707 (1966).
16. Teo, B. K., and Lee, P. A., *J. Amer. Chem. Soc.* **101,** 2815 (1979).
17. Hoekstra, H. R., Siegel, S., and Gallagher, F. X., *Adv. Chem. Ser.* **98,** 41 (1971).
18. Lytle, F. W., *J. Catal.* **43,** 376 (1976).
19. Lytle, F. W., Wei, P. S. P., Greegor, R. B., Via, G. H., and Sinfelt, J. H., *J. Chem. Phys.* **70,** 4849 (1979).
20. Gallezot, P., Weber, R., Dalla Betta, R. A., and Boudart, M., *Z. Naturforsch. A* **34,** 40 (1979).
21. Mansour, A. N., Cook, J. W., Sayers, D. E., Emrich, R. J., and Katzer, J. R., submitted for publication.
22. Short, D. R., Mansour, A. N., Cook, J. W., Sayers, D. E., and Katzer, J. R., submitted for publication.
23. Tauster, J. J., Fung, S. C., and Garten, R. I., *J. Amer. Chem. Soc.* **100,** 170 (1978).
24. Horsley, J. A., *J. Chem. Phys.* **76,** 1451 (1982).
25. Lytle, F. W., Greegor, R. B., Marques, E. C., Biebesheimer, V. A., Sandstrom, D. R., Horsley, J. A., Via, G. H., and Sinfelt, J. H., "Determination of the Atomic and Electronic Structure of Pt Catalysts by X-Ray Absorption Spectroscopy," presented at ACS National Meeting, Philadelphia, August, 1984. To be published in "New Surface Science in Catalysts," ACS Symposium Series.